Raman spectroscopic analysis of human skin tissue sections *ex-vivo*: evaluation of the effects of tissue processing and dewaxing

Syed M. Ali
Franck Bonnier
Ali Tfayli
Helen Lambkin
Kathleen Flynn
Vincent McDonagh
Claragh Healy
T. Clive Lee
Fiona M. Lyng
Hugh J. Byrne

Raman spectroscopic analysis of human skin tissue sections *ex-vivo*: evaluation of the effects of tissue processing and dewaxing

Syed M. Ali,[a] Franck Bonnier,[a] Ali Tfayli,[b] Helen Lambkin,[c] Kathleen Flynn,[c] Vincent McDonagh,[d] Claragh Healy,[d] T. Clive Lee,[d] Fiona M. Lyng,[a] and Hugh J. Byrne[e]
[a]Dublin Institute of Technology, Radiation and Environmental Science Centre, Focas Research Institute, Kevin Street, Dublin 8, Ireland
[b]Univ Paris-Sud, GCAPS "Groupe de Chimie Analytique de Paris-Sud", Faculty of Pharmacy, 92290 Chatenay Malabry, France
[c]Institute of Technology, School of Biological Sciences, Dublin Kevin Street, Dublin 8, Ireland
[d]Royal College of Surgeons in Ireland, Department of Anatomy, 123 St. Stephen's Green, Dublin 2, Ireland
[e]Dublin Institute of Technology, Focas Research Institute, Kevin Street, Dublin 8, Ireland

Abstract. Raman spectroscopy coupled with K-means clustering analysis (KMCA) is employed to elucidate the biochemical structure of human skin tissue sections and the effects of tissue processing. Both hand and thigh sections of human cadavers were analyzed in their unprocessed and formalin-fixed, paraffin-processed (FFPP), and subsequently dewaxed forms. In unprocessed sections, KMCA reveals clear differentiation of the stratum corneum (SC), intermediate underlying epithelium, and dermal layers for sections from both anatomical sites. The SC is seen to be relatively rich in lipidic content; the spectrum of the subjacent layers is strongly influenced by the presence of melanin, while that of the dermis is dominated by the characteristics of collagen. For a given anatomical site, little difference in layer structure and biochemistry is observed between samples from different cadavers. However, the hand and thigh sections are consistently differentiated for all cadavers, largely based on lipidic profiles. In dewaxed FFPP samples, while the SC, intermediate, and dermal layers are clearly differentiated by KMCA of Raman maps of tissue sections, the lipidic contributions to the spectra are significantly reduced, with the result that respective skin layers from different anatomical sites become indistinguishable. While efficient at removing the fixing wax, the tissue processing also efficiently removes the structurally similar lipidic components of the skin layers. In studies of dermatological processes in which lipids play an important role, such as wound healing, dewaxed samples are therefore not appropriate. Removal of the lipids does however accentuate the spectral features of the cellular and protein components, which may be more appropriate for retrospective analysis of disease progression and biochemical analysis using tissue banks. © *2012 Society of Photo-Optical Instrumentation Engineers (SPIE).* [DOI: 10.1117/1.JBO.18.6.061202]

Keywords: Raman spectroscopy; K-means cluster analysis; human skin tissue; hand; thigh; tissue dewaxing; keratinocytes; melanin; collagen; lipids; wound healing; biochemical analysis.

Paper 12269SS received May 2, 2012; revised manuscript received Jul. 11, 2012; accepted for publication Jul. 12, 2012; published online Nov. 2, 2012.

1 Introduction

Vibrational spectroscopic techniques, both infrared absorption and Raman scattering, have been widely used for the study of biological samples over the past two decades. The main advantages of these techniques are that they provide a non invasive, label free molecular fingerprint of the tissue and cells. Their potential in medical diagnostics has been well demonstrated and many further reaching applications have been described, including those in radiobiology,[1] toxicology,[2] and pharmacokinetics.[3] Coupled with adapted multivariate analysis, the specificity of the information obtained can be used for the identification of different pathologies,[4,5] or variations in metabolism as a result of external agents[6,7] and even subcellular analysis.[8,9]

In the past, many studies have been carried out using vibrational spectroscopy to classify tissue for cancer diagnosis. Some of the tissue types examined by various groups include cervical,[10,11] lung,[12,13] brain,[14] esophagus,[15–17] colon,[18,19] prostate,[20] nasopharynx,[21] larynx,[22] oral,[23] breast,[24–27] and liver.[28] In dermatological research, Fourier transform infrared (FTIR) spectroscopy has been employed for tumour detection in colon and skin biopsies.[5,29,30] Raman spectroscopy has been demonstrated to provide an accurate diagnosis to distinguish basal cell carcinoma from surrounding normal tissue[31–33] and can also be used as an efficient tool for examination of skin biochemical structure and content[34,35] of interest for dermal application of cosmetic and pharmacological agents.

A variety of different methods of sample preparation have been employed in these studies: fresh, frozen, air dried, formalin-fixed, paraffin-processed (FFPP), and subsequently dewaxed tissue sections. Although considered the gold-standard, fresh or unprocessed skin tissue is difficult to obtain and sectioning can be a delicate task. Embedding in paraffin wax is commonly undertaken to preserve the samples before histological analysis.[36,37] Archived embedded tissue banks potentially serve as a significant resource for retrospective prognosis studies.

For clinical relevancy, and indeed acceptance of the techniques by the clinical community, it is important that the sample

preparation protocols for Raman spectroscopic analyzes are consistent with current practice. The embedding wax itself can, however, contribute significantly to the spectroscopic signature[38] and although "digital dewaxing" has been demonstrated,[39] it is often important to compare spectroscopic profiling with parallel histological analyzes of dewaxed sections. It is critical however to consider the effects of tissue processing on the biochemical integrity of the tissue structures. Cell fixation has been demonstrated to impact the spectroscopic signatures of cell populations,[40–42] and commonly employed tissue processing techniques have been shown to have similar effects.[38]

In this study, Raman spectroscopy is employed to characterize the biochemical profile of sections of unprocessed human tissue. The layer structure is characterized by comparison to pure biochemical components and keratinocyte cell lines, and the relative morphologies and biochemical content of sections from human hand and thigh are compared. The sections are subsequently dewaxed using standard clinical protocols, and the spectral analysis is repeated. It is demonstrated that the tissue processing has significant impact on the extracellular structure, notably the lipidic content, such that tissue sections from different anatomical sites are no longer distinguishable. In the processed tissue sections, however, the decreased lipidic content renders the cellular and extracellular protein structures more distinct, which is potentially advantageous for retrospective analysis of disease progression and biochemical analysis using tissue banks.

2 Materials and Methods

2.1 Tissue Samples

Skin tissue was provided through the Anatomical Gift Programme of the Royal College of Surgeons of Ireland (RCSI). Details of the cadaver samples available for this study are provided in Table 1. Skin samples were collected from 11 human cadavers. In each case, both dorsal (back) hand and proximal,

Table 1 Human cadavers. Spectral profiling of hand and thigh sections, unprocessed and processed, of the samples indicated by shading are presented in detail.

Identification no.	Sex	Age	Cause of death
Sample no 1	Female	82	Pancreatic malignancy
Sample no 2	Female	98	Bronchopneumonia
Sample no 3	Female	88	Myocardial infarction
Sample no 4	Female	88	Small bowel obstruction
Sample no 5	Female	89	Cerebrovascular accident
Sample no 6	Female	78	Bronchopneumonia
Sample no 7	Female	93	Urinary tract infection
Sample no 8	Male	77	Chronic obstructive pulmonary disease
Sample no 9	Male	89	Cerebrovascular accident
Sample no 10	Male	81	Myocardial infarction
Sample no 11	Male	73	Motor neuron disease

medial thigh sections were employed, and each sample was measured in unprocessed, formalin-fixed, paraffin-embedded (FFPP), and subsequently dewaxed form. All samples are preserved at $-80°C$ before cutting and analysis. Unprocessed cross-sections of 20 μm thickness were cut with a cryomicrotome (LeicaCM 1850 UV) and were stored at $-20°C$ until used. Spectral profiling of hand and thigh sections, unprocessed and processed, of the samples indicated by shading in Table 1 are presented in detail.

The skin tissue was automatically processed (Leica Histokinette 2000) to wax blocks using four principle steps, as follows:

(1) Vacuum fixation in 10% buffered formal saline histograde pH 6.8 to 7.2 (J. T Baker, Deventer, the Netherlands) and heating to 30°C.

(2) Vacuum dehydration in industrial methylated spirit industrial methylated sprit T100 (Lennox, Dublin Ireland).

(3) Vacuum clearing in xylene (Serosep, Limerick, Ireland) and heating to 35°C.

(4) Vacuum impregnation with tissue 111 Embedding Wax with polymer added (Sakura, Zoeterwoude, the Netherlands) and heating to 59°C.

After wax impregnation, tissue was embedded and sliced into 20 μm sections using a microtome, mounted on a CaF_2 substrate and dried. The samples were immersed in a series of baths consisting of two baths of xylene (British Drug Houses, Dorest, UK) for 5 and 4 min, respectively, two baths of Ethanol Absolute (Merck, Dorest, UK) for 3 and 2 min, and a final bath of Industrial Methylated spirits 95% (Lennox Dublin, Ireland) for 1 min.

2.2 Cell Cultures

HaCaT cells are spontaneously immortalized human epithelial keratinocytes derived from adult skin, and have the characteristics of basal epidermal keratinocytes.[43] This cell line can be used as an *in vitro* model for highly proliferative epidermis.[44]

HaCaT cells were cultured in Dulbecco's Modified Eagle Medium (DMEM) F12 (1:1) medium (Sigma, Dorset, UK) containing 10% fetal calf serum (Gibco, Irvine, UK), 1% penicillin-streptomycin solution 1000 IU (Gibco, Irvine, UK), 2mM L-glutamine (Gibco, Irvine, UK), and 1 μg mL^{-1} hydrocortisone (Sigma, Dorset, UK) in a humidified atmosphere containing 5% CO_2 at 37°C. HaCaT cells were seeded at a concentration of 4×10^4 cells per substrate onto CaF_2 substrate (Hellma Ltd., UK), previously sterilized using ethanol then dried in a laminar flow. All samples were incubated for 24 h at 37°C, 5% CO_2 before measurement. Cells were measured live, in NaCl solution, using the LUMPlanF1, Olympus immersion objective.

2.3 Biochemical Compounds

For comparison to tissue spectra, a number of biochemical compounds were analyzed by Raman spectroscopy. The samples were purchased from Sigma-Aldrich (Ireland). Samples of ceramide, sphingomyelin, and L-α-phosphatidylcholine (1,2-Diacyl-sn-glycero-3-phosphocholine, 99% from egg yolk) were dispersed in chloroform, and small amounts of material were drop cast onto CaF_2 substrates.

2.4 Raman Instrumentation

A Horiba Jobin-Yvon LabRAM HR800 spectrometer with an external 300 mW diode laser operating at 785 nm as source was used throughout this work. For the measurements, either a ×100 objective (MPlanN, Olympus) or a ×100 immersion objective (LUMPlanF1, Olympus) was employed, each providing a spatial resolution of ~1 μm at the sample. The confocal hole was set at 100 μm for all measurements, the specified setting for confocal operation. The system was spectrally calibrated to the 520.7 cm^{-1} spectral line of silicon, and the intensity response function was corrected using the Standard Reference Material (SRM) No. 2243 of the National Institute of Standards, Boulder, Colorado, USA (NIST SRM 2243, 2242, 2241).[45] The Labram system is a confocal spectrometer that contains two interchangeable gratings (300 and 900 lines/mm, respectively). In the following experiments, the 300 lines/mm grating was used, giving a spectral dispersion of ~1.5 cm^{-1} per pixel. The detector used was a 16-bit dynamic range Peltier cooled CCD detector. A step size of 2 μm was employed for tissue mapping.

Tissue samples were measured under water immersion to minimize the spectral background, and spectra were recorded using the immersion objective (LUMPlanF1, Olympus).[46] All biochemical samples were recorded using the ×100 objective (MPlanN, Olympus). Once all spectra were acquired, a background of substrate measured under identical conditions was subtracted. Minimal baseline correction, smoothing, and normalization were also performed in order to improve the quality of the acquired spectra.

2.5 Data Analysis

The different data analysis steps were performed using Matlab (Mathworks, USA). Before statistical analysis, a Savitsky-Golay filter (5th order, 7 point) was applied to smooth any spurious peaks of the spectra and reference constituting the background signal.

K-means cluster analysis (KMCA) was employed to analyze the spectral variations in tissue. It is one of the simplest unsupervised learning algorithms that solves the well known clustering problem and is often used for spectral image analysis.[19] In general, clustering is the partitioning of a data set into subsets (clusters) so that the differences between the data within each cluster are minimized, and the differences between clusters are maximized according to some defined distance measure. Using KMCA, the large amount of data in a spectral map can be reduced to mean spectra, and the spatial distribution can easily be visualized. The Raman data were used as inputs for KMCA. The clustering analysis algorithm was used to find groups of spectra with similar spectral characteristics (clusters), each one representing regions of the image with similar biochemical profiles. After KMCA, a different color is assigned to each cluster. Each grid element of the spectral map is then assigned the color of the particular cluster to which its spectrum belongs. In this way, a pseudo-color image of the skin sections is created to visualize the organization of the clusters in the original image. As the tissue mapping step size was 2 μm for all measurements, pixel size in the KMCA maps is 2 μm × 2 μm. The data range for all KMCA was limited to the fingerprint region, 400 to 1800 cm^{-1}.
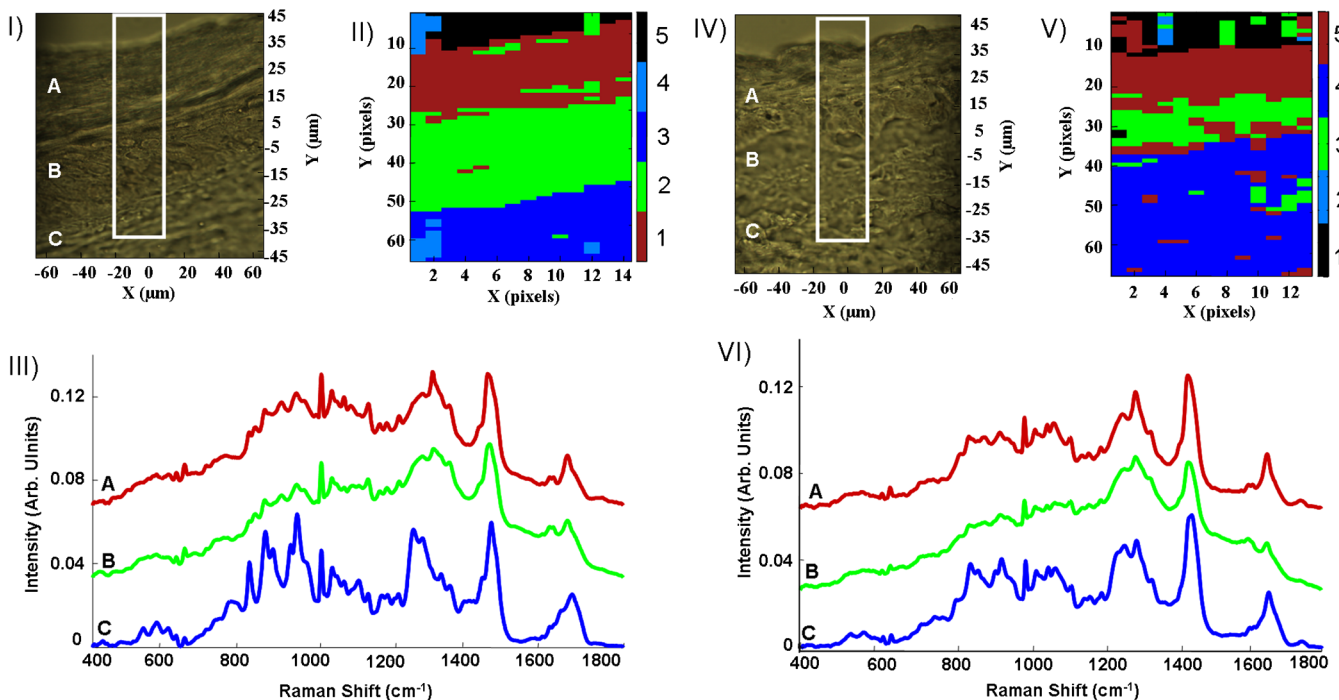

Fig. 1 (a) Optical image of unprocessed hand tissue section; (b) K-means cluster analysis of Raman maps of unprocessed hand; (c) KMCA mean Raman spectra of unprocessed hand illustrating the differentiation of the superficial stratum corneum (SC; cluster 1 = A), the intermediate epithelium (cluster 2 = B), and the dermis (cluster 3 = C); (d) Optical image of unprocessed thigh tissue section; (e) K-means cluster analysis of Raman map of unprocessed thigh; (f) KMCA mean Raman spectra of unprocessed thigh, illustrating the differentiation of the superficial SC (cluster 5 = A), the underlying epithelium (cluster 3 = B), and the dermis (cluster 4 = C).

3 Results and Discussion

3.1 Identification of the Different Skin Layers in Unprocessed Samples

Figure 1(a) shows an optical microscopic image of a 20 μm thick, unprocessed hand section of sample no. 3. Visually, three different regions are apparent. Raman and FTIR spectroscopy, coupled with KMCA, can be used for the identification of different structures and classification of tumoral regions in tissue sections.[29,47] It may, therefore, be anticipated that distinct biochemical regions within the skin section can be identified. The maximum biochemical information is contained within the so-called fingerprint region of the spectrum (400 to 1800 cm^{-1}) and therefore this region was initially analyzed. In an automated spectral map of the tissue sections, the spectra recorded on the edge of the tissue exhibit a high degree of variability due to the transition from the outer layer of tissue to the substrate. The variability between these spectra can interfere with the clustering analysis, resulting in the creation of distinct clusters. Best visualization and reproducibility of the different structures existing within the tissue was achieved by setting the number of clusters to five. In this way, the variability in the spectra obtained at the edge of the tissue is contained in distinct clusters and does not interfere with the identification of different structures present in the tissue. The spectra were assigned to the five different groups according to their similarities, and a color was attributed to each cluster. False color maps were constructed representing the partition of the different clusters in the tissue. The resulting image can be seen in Fig. 1(b).

Three different structural layers can be found in the skin: the epidermis, the dermis, and hypodermis. The latter is too deep to be sampled *in vivo* using Raman microscopy and is not examined in this study. The epidermis forms the protective layer against the surrounding environment. The dermis provides a structural support to the skin, and the hypodermis is a connective tissue layer where fat is stored. The epidermis can also be subdivided into four different layers, starting with the stratum basale, adjacent to the dermis, containing mainly keratinocytes but also melanocytes responsible for the production of melanin, a pigment which protects against ultraviolet (UV) radiation. The second layer is called the stratum spinosum and is formed from dividing basale cells migrating towards the surface of the skin. The third layer is named the stratum granulosum and is characterised by anuclear cells. As a natural process of maturation, the cells flatten and lose their nucleus. Finally, in contact with the exterior environment, is the SC. The cells have reached the last stage of their maturation and are described as non-viable, cornified cells, called corneocytes. A fifth layer, the stratum lucidum, is found in the sole of the foot and palm of the hand and is therefore not present in our samples.

Three different regions of skin can be well differentiated spectroscopically, and Fig. 1(c) shows KMCA mean spectra related to the three regions of unprocessed hand derived from the subsection of Fig. 1(a) (indicated by the white rectangle). Of the other two clusters identified, the black (cluster 5) corresponds to the substrate, while the light blue (cluster 4) in Fig. 1(b) is not associated with specific skin structure and represents either a loss of layer integrity during the sectioning process or presence of debris on the substrate. Nevertheless, the specificity of the information contained in the spectra recorded allows discrimination of different skin layers using KMCA. Analysis of a thigh tissue section yields similar results, as shown in Fig. 1(d), 1(e), and 1(f).

Notably, in both cases, the number of layers found is less than that of the skin anatomy described above. It is thus of interest to analyze the spectral features which differentiate these layers of skin, as well as skin from different anatomical sites and elucidate the biochemical origin of their differentiation.

3.2 Characterization of the Dermal Layer

Figure 2(a) presents a comparison between the KMCA cluster 3 mean spectra for unprocessed hand and the equivalent cluster for thigh [see A and B in Fig. 2(a)] with pure collagen [see C in Fig. 2(a)]. It can be easily seen that the spectrum of the skin layer is dominated by collagen, and it is therefore identified
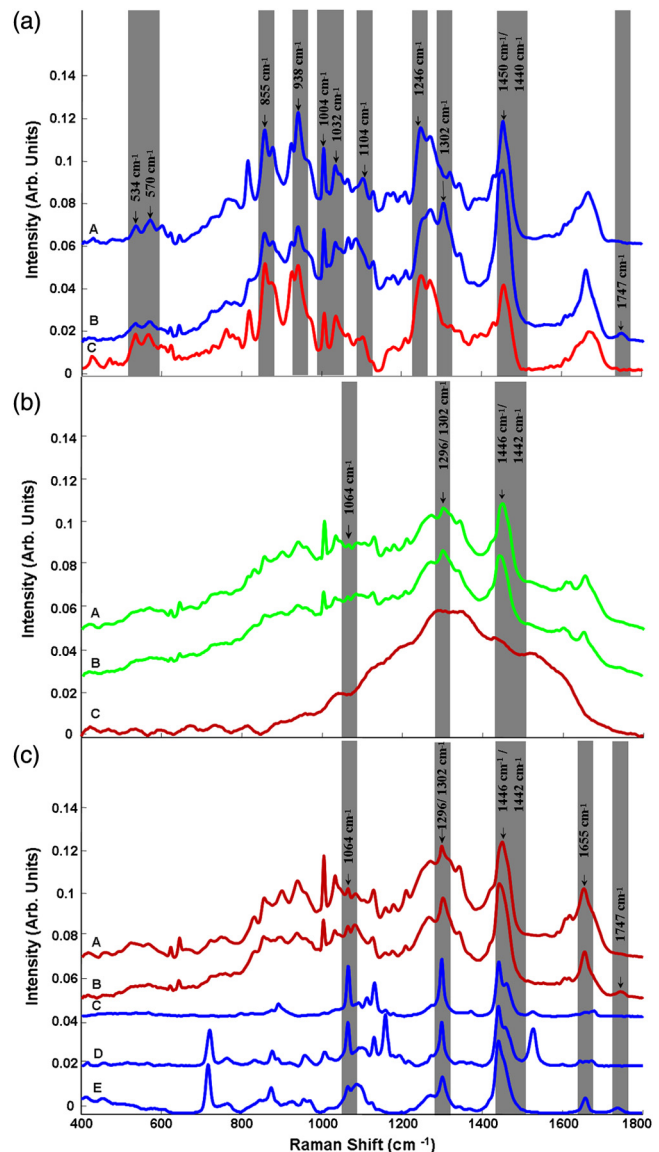

Fig. 2 (a) KMCA mean spectra of unprocessed hand skin dermis cluster (cluster 3) (A), unprocessed thigh skin dermis cluster (cluster 4) (B), and spectrum of pure collagen (C); (b) KMCA mean spectra of the intermediate epithelial layer cluster (cluster 2) of unprocessed frozen hand skin (A), the intermediate epithelial layer cluster (cluster 3) of unprocessed thigh skin (B), and spectrum of pure melanin (C); (c) KMCA mean spectra of the SC cluster (cluster 1) of unprocessed hand (A), the SC cluster (cluster 5) of unprocessed thigh (B), spectra of Ceramide (C), Sphingomyelin (D), and L-α-phosphatidylcholine (E).

as the dermis. This is due to the high composition of collagen in human dermis, constituting about 70% of the dry weight and 90% of the total protein content. There are about 20 types of collagen that exist in the body, but 80% of skin collagen is Type 1 and 15% is Type 3. The remaining 5% is thought to be predominately Type IV collagen.[48–50]

Assignments of most Raman bands of collagen have been made by Frushour and Koenig.[51] Specific features in the collagen spectrum are two intense bands at ~855 and ~938 cm^{-1}. These bands originate from the amino acid side chain vibrations of proline and hydroproline as well as from a C–C stretching vibration of the collagen backbone. Proline and hydroxyproline make up about one fourth of the amino acids in collagen, a higher proportion than in most other proteins.[48] More generic protein bands present in the spectrum of the collagen and the dermis appear at 1452 cm^{-1}, 1104 cm^{-1} due to CH deformation and C–N stretching, while features at 1004 and 1032 cm^{-1} are due to symmetric ring breathing and CH in-plane bending (phenylalanine).[52–56] These bands are also evident in the mean spectra of the other layers, but the collagen specific peaks are absent, and they are thus distinctive signatures of the dermal layer.

3.3 Characterization of the Epidermal Layers

Overlaying the dermis, KMCA of the Raman maps identify two epidermal layers, although the anatomy of the epidermis divides it into four distinct layers. Analysis of the spectral information elucidates the origin of the subclassification.

Figure 2(b) displays a comparison between the KMCA cluster 2 mean spectrum of unprocessed hand (A) and the equivalent mean spectrum of unprocessed thigh (B) skin section corresponding to the intermediate epidermal layer with the spectrum of pure melanin (C). The pure melanin spectrum [see C in Fig. 2(b)] is dominated by the broad fluorescence emission spectrum, and no prominent Raman peaks are apparent. The spectra of the intermediate layers of unprocessed hand and thigh skin [see A and B in Fig. 2(b)] are a superposition of the fluorescence spectrum of melanin itself and the spectrum of the extracellular matrix present in the dermis of the skin. The basal layer of the epidermis is primarily composed of melanocytes, which are responsible for the production of melanin. Melanin is one of the most ubiquitous and biologically important pigments in the human body.[57] Although melanin is produced by melanocytes, the pigment accumulates in melanosomes which are transferred to the adjacent keratinocytes where they remain as granules. Thus, the melanin is distributed beyond the basal layer and can be found in the entire malpighian layer, a term that can be used to collectively describe the stratum spinosum and granulosum.[58,59] The organization and distribution of the melanin vary between individuals and in darkly pigmented skin, even the corneocytes can contain specks of melanin also described as "dust." However the number of melanocytes is relatively constant.[57]

Because of the pigmented nature, the cluster spectra show a strong background, potentially due to the fluorescence of the melanin, which is resonant at 785 nm,[60] although distinct Raman peaks can be clearly identified. As a result, the intensity of the spectrum is also exceptionally high. The presence of a strong background in the spectra does not allow to specifically discriminate the basal layer from the malpighian layer, and KMCA of the Raman map identifies the combination as an intermediate epithelial layer. An increase in the cluster number to 7 or 10 differentiates more "outlier" regions associated with the interface between sample and substrate, indicating that the variations in this region are larger than those in the intermediate layer, dominated by the melanin fluorescence. The strong background in the Raman spectrum makes it difficult to quantify the melanin levels based on Raman spectroscopy. Moreover, these layers, being mostly composed of keratinocytes, albeit at different stages of maturation, are more likely to be spectroscopically very similar.

Most of the Raman bands in the KMCA spectrum of cluster 1 for unprocessed hand and the equivalent cluster for thigh sections are in agreement with results obtained from FT-Raman measurements on isolated SC.[61–64] The SC spectra are dominated by contributions from keratin and lipids. Figure 2(c) represents a comparison between the Raman spectra of the KMCA cluster 1 for unprocessed hand (A) and the equivalent cluster for unprocessed thigh (B) with spectra of the pure lipids ceramide (C), sphingomyelin (D), and L − α-phosphatidylcholine (E). The position of the amide I band at 1655 cm^{-1} indicates that keratin in the human SC adopts predominantly an α-helical conformation.[65,66] Additionally, the spectra of cluster 1 hand and the equivalent for thigh have prominent contributions of lipids, observed at 1064, 1085, and 1130 cm^{-1} due to chain C–C stretching, 1296 and 1302 cm^{-1} due to CH$_2$ twisting, as well as 1446 and 1442 cm^{-1} due to CH scissoring. All bands can be compared to strong features in the Raman spectra of ceramide, sphingomyelin, or phosphatidylcholine. However, the most abundant classes of lipids present in the SC are ceramide, cholesterol, and fatty acids, wherein they play a pivotal role in the skin barrier function. The absence of the intense Raman features at 717, 1157, and 1526 cm^{-1} clearly highlights that sphingomyelin is absent from the SC. Similarly, the absence of a strong peak at 717 cm^{-1} in the spectrum of the skin seems to indicate that no contribution from the phospholipids can be observed. However the presence of a small feature at 1747 cm^{-1} remains identifiable. The exact lipidic composition of the SC remains difficult to evaluate. The presence of sebaceous lipids, composed of squalene, wax esters, and triglycerides, coating the skin surface can be a result of contamination during sample preparation.[67] However, in recent studies, the SC is commonly described as mostly composed of ceramides, fatty acids, and cholesterol although other lipids may be present in small quantities. Earlier studies indicated that phospholipids in the SC account for about 5% of the total lipids from samples taken from the legs or abdomen but smaller proportions in other locations such as the face.[68–70]

The absence of characteristic features of carotenoids in the SC is also notable. The distribution of these powerful antioxidants in the skin was recently investigated in vivo using Raman microscopy based on the prominent Raman line at 1525 cm^{-1} (C = C vibration).[71–73] It is assumed that they are degraded due to the oxidative stress induced by death.

Raman spectroscopy, coupled with KMCA, is clearly a powerful tool to differentiate the layers of skin, as well as layers from different anatomical sites, based on biochemical content. The images reveal significant differences between the morphology and thickness of the SC and basal layer of the two different anatomical sites. Using the false color images reconstructed from the KMCA, the dermis can be easily differentiated due to the high content of collagen, and therefore the delimitation between the dermis and the epidermis is easily discernable. The two remaining clusters are attributed to the SC

and an intermediate combination of the basal and malpighian layers. Across the sections of unprocessed hand examined, the total thickness of the epidermis appears to be about $70 \pm 15 \mu$m whereas in the thigh sections it is within the range $35 \pm 5 \mu$m. Although the thicknesses vary somewhat from sample to sample, these differences between sections of hand and thigh are consistent across samples from all 11 cadavers measured. The cluster identified as the top layer of the skin without any features of the melanin can be attributed to the SC, and was found to be respectively $40 \pm 10 \mu$m for the unprocessed hand and $25 \pm 5 \mu$m for the thigh.

Epidermal thickness is of considerable significance in dermatological research and a considerable amount of work has been done and reported, both *in vivo*[74,75] and *ex vivo* from biopsy samples,[76–78] defining the variations of epidermal thickness of different anatomical sites. The observations here are consistent with those expected for primarily sun-exposed sites (hand) and sun-protected sites (thigh). It has also been observed that the degree of variability on normally clothed body sites is less than that on the normally unclothed sites.[79] Variations in normal skin related to age and gender have also been reported.[77] Published values of the thickness of the viable layer (basal layer) and the SC have been variable. Moreover, the thickness of SC and other layers of the epidermis are known to be different from different anatomical sites. In recent studies, the total thickness has been found to be between 60 and 100 μm depending on the body sites considered, but more importantly the techniques employed for the measurements.[80,81] However, less is known about the biochemical differences, and Raman spectroscopic analysis can potentially shed further light on chemical differences between the skin layers, and between layers from different anatomical sites. Important for generalization of deductions is the consistency of the differentiation between specimens. Figure 3(a) and 3(b) compares the average spectra of the epidermis of unprocessed hand and thigh sections from different anatomical sites. The results are representative of all 11 cadaver measured samples.

The samples available for this study have been taken post-mortem from patients over 80 years (Table 1). The thickness of the different skin layers can be affected by aging or sun exposure and therefore can vary significantly from individual to individual. The observations made can thus not be considered to be representative of the whole population. However, as the samples have been taken from different locations (hand and thigh) for each cadaver, direct comparison between two samples from the same patient remains relevant.

Spectra of the SC and dermis of different individuals show strong similarities, but some structural and conformational differences are apparent, as illustrated in Fig. 3(a) and 3(b). Overall, the Raman signatures vary significantly and consistently according to body site (hand and thigh). Apparent shifts in the features at 1446/1442 and 1296/1302 cm^{-1} are consistently observed from thigh to hand SC (Fig. 3). The relative intensity of the signal at 1296 and 1302 cm^{-1} with respect to the peak at 1266 cm^{-1} also varies. Similar differences are observed between unprocessed hand and thigh sections in the case of the intermediate epithelial layer [Fig. 2(b)] and the dermis [Fig. 3(b)]. The band located at 1302 cm^{-1} in thigh dermis [Fig. 3(b)] is assigned to CH$_2$ twisting, and this is absent in hand dermis, while the Amide III band located at 1246 cm^{-1} in hand dermis is absent in thigh dermis. Figure 3 illustrates that these are regions of strong lipid contributions, however,
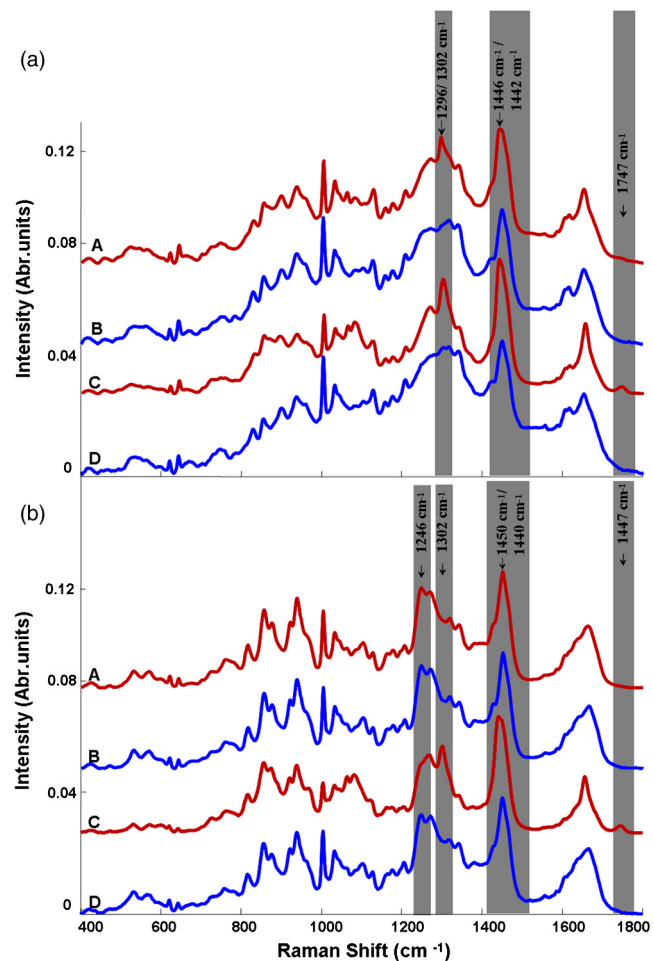

Fig. 3 (a) A: Average Raman spectrum of the unprocessed hand SC; B: Average Raman spectrum of the dewaxed hand SC; C: Average Raman spectrum of the unprocessed thigh SC; D: Average Raman spectrum of the dewaxed thigh SC. (b) A: Average Raman spectrum of the unprocessed hand dermis; B: Average Raman spectrum of the dewaxed hand dermis; C: Average Raman spectrum of the unprocessed thigh dermis; D: Average Raman spectrum of the dewaxed thigh dermis.

and so, rather than spectral shifts, these characteristic differences are more likely due to differing contributions of lipids to the spectra relative to those of proteins.

Thigh SC and dermis also display a small peak at 1747 cm^{-1}, which is absent from hand SC and dermis. This peak is evident in the spectrum of L-α-phosphatidylcholine [see E in Fig. 2(c)] and derives from the C = O ester vibration, also present in triglycerides, which are not normally present in the SC. Triglycerides are esters derived from glycerol and three fatty acids, and their prominence in the thigh tissue may be evidence of higher levels of lipids and fatty acids.

3.4 Study of the CH Region

Differences in lipidic content of the different layers can be more clearly visualized in the high wavenumber region of the Raman spectrum, in which the CH vibrations of the aliphatic chains feature strongly. Figure 4 presents a comparison between the average, baseline corrected, Raman spectra of unprocessed SC (A), unprocessed intermediate layer (B), unprocessed dermis (C) in
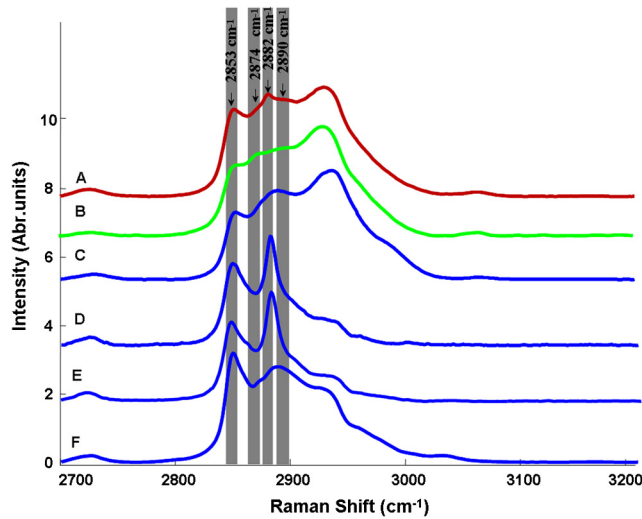
Fig. 4 Average Raman spectra of high wavenumber region of unprocessed thigh SC (A), unprocessed intermediate epithelial layer (B), unprocessed dermis (C), ceramide (D), sphingomyline (E), and L-α-phosphatidylcholine (F).

Table 2 Fitted peak positions, relative intensities and assignments for the high wavenumber region of average Raman spectra of unprocessed skin sections.

Peak position (cm^{-1})		Stratum corneum	Dermis	Intermediate epithelium	Assignment
Thigh	2730	0.12	0.08	0.07	CH stretching (lipid)
Hand		0.06	0.05	0.02	
Thigh	2850	0.73	0.56	0.80	CH$_2$ stretching (lipid)
Hand		0.65	0.24	0.65	
Thigh	2863	0.67	0.43	0.73	CH$_3$ stretching (protein)
Hand		0.70	0.45	0.59	
Thigh	2880	0.42	0.46	0.03	CH$_2$ stretching (lipid)
Hand		0.13	0.08	0.002	
Thigh	2905	1.03	0.93	1.16	CH stretching (protein)
Hand		0.80	0.67	0.94	
Thigh	2933	1	1	1	CH$_3$ stretching (protein)
Hand		1	1	1	
Thigh	2968	0.59	0.50	0.82	CH$_3$ stretching (protein)
Hand		0.50	0.53	0.64	
Thigh	3065	0.05	0.03	0.07	Amide B (protein) (CNH bend)
Hand		0.05	0.06	0.07	

the region from ~2700 to ~3200 cm^{-1}, compared with pure ceramide (D), sphingomyline (E), and L-α-phosphatidylcholine (F). The strong contributions of the lipids can be seen clearly in the spectra of all three layers of the frozen skin section, although their relative contributions vary. The spectra can be fitted with individual Gaussian/Lorentzian bands, and the results are summarized in Table 2. Spectral positions of the fitted peaks vary somewhat from spectrum to spectrum, and so are quoted ± 3 cm^{-1}. Fitted peak intensities are reproducible within 10% and are normalized to the band at ~2932 cm^{-1}. The peaks in the high number region predominantly originate from CH, CH$_2$, and CH$_3$ stretching, and from literature, many can be assigned to lipids, the remainder being assigned to proteins.[34,35,82,83]

In general, the SC is seen to be relatively rich in lipidic content, essential for the barrier function of the skin against external agents. The SC is made up of keratinized cells that are embedded in lipid matrices like bricks in mortar,[84] or more specifically corneocyte cells surrounded by a three-dimensional, multi-lamellar lipid domain.[85,86] As part of the cell maturation, the keratinocytes' enzymes degrade the cellular viable components such as nucleus and other organelles. Therefore, corneocytes are anucleated cells, and no DNA or histones should be found in this layer of the skin. The major lipid components of the SC are ceramides (sphingosines and phytosphingosines), long-chain free fatty acids, and cholesterol.[87–90]

The main lipids in the basal layer are phospholipids, cholesterol, and to a lesser extent triglycerides, which provide energy for metabolism. The lipids are subject to maturation, and it starts with the apparition of lamellar bodies in the stratum spinosum which contain phospholipids, sphingolipids, and cholesterol.[91] The lamellar granules present in the stratum granulosum are particularly rich in glucosylceramides. These granules are released in the intercellular space of the SC where they will be converted into ceramides via hydrolysis by beta (b)-glucocerebrosidase.[92,93]

Overall, it can be deduced that lipid/protein compositions are not uniform in the layers of hand and thigh of the same human cadavers. The sun-exposed hand skin is relatively low in lipidic

content compared to the thigh. This is consistent with reports that a decrease in lipid content is associated with increased susceptibility to exogenous insults, which will naturally increase with age.[94] The observations may provide unique advantages in skin disease diagnosis, and this body-site difference needs to be factored into *in vivo* skin Raman assessment and disease diagnosis. However, it is noted that for both anatomical sites, the Raman spectra of the SC and dermis of skin sections are strongly influenced by the lipidic and extracellular protein content, rather than the cellular features, which may provide the most direct biochemical information on tissue pathology. Raman spectroscopy can be used, not only to elucidate the structure of the lipids involved in the SC barrier function (ceramides, cholesterol, and free fatty acids), but also to provide a direct insight on the conformational order and the lateral packing of these lipids. It has been shown that the barrier function is directly related to the compactness of the lipid structure and that the later can be affected by external insults such as UV radiation.[35,95–97]

3.5 Comparison with Processed FFPP Sections

For histological analysis, tissue samples are commonly preserved in paraffin wax.[36,37] Paraffin embedding facilitates tissue cutting, but also is commonly employed, worldwide, for

archiving tissue samples. The availability of a wide range of pathologically characterized samples for study potentially enables extensive retrospective studies using spectroscopic and other techniques. However, the paraffin wax itself gives rise to strong Raman signals that overlap the molecular vibrations of the biomolecules of the samples, necessitating chemical removal for spectral analysis.[38] Although it has been demonstrated that the contributions can be removed digitally,[98] histological staining, considered a gold standard, necessitates chemical removal of the wax, and thus the procedure is employed here. Furthermore, although it has been demonstrated that dewaxing using hexane is more efficient than the commonly employed xylene, xylene is used here for consistency with clinical protocols.[38]

Figure 5(a) shows an optical microscopic image of the dewaxed hand section of human skin of 20 μm thickness. As for the unprocessed sections, three different regions are visually apparent, the dermis at the bottom and the SC at the top, separated by an intermediate underlying epidermal layer. In contrast, the optical images of dewaxed hand and thigh skin sections in Fig. 5(a) and 5(d) indicate no major differences between the thicknesses of the total epidermis, which are ∼40 μm in both thigh and hand. The SC also appears to have similar thicknesses in both locations, ∼20 μm, despite the large differences observable in the unprocessed sections from the same cadavers. Through the processes of formalin-fixation, paraffin-embedding, and dewaxing, as well as cutting, the tissue sections likely undergo a considerable degree of chemical and physical changes, and it is important to consider the effects of the processing on the biochemical content and structure of the skin layers.

Spectroscopically, the three regions of the sections are quite distinguishable, as illustrated by the KMCA mean spectra of Fig. 5(c), taken within the subsection of Fig. 5(a) indicated by the white rectangle. The KMCA map of Fig. 5(b) further supports classification of dermis, basal/malpighian layer, and SC. The mean spectra of the principle regions are plotted in

Fig. 5(c). The mean spectrum of cluster 4 is similar to that of cluster 1. Similar results are observed for dewaxed thigh tissue sections and are shown in Fig. 5(d), 5(e), and 5(f). For both anatomical sites, at first glance, the mean spectra of the three identified regions are similar to the corresponding regions for the unprocessed skin sections, but closer examination reveals important differences.

Figure 6(a) presents a comparison between the spectra of KMCA cluster 1 of dewaxed skin hand SC (A) and the equivalent cluster of dewaxed thigh SC (B) with that of the HaCaT cell line (C), DNA (D), histone (D), and pure paraffin wax (F). Firstly, it is noted that the KMCA spectra of dewaxed epidermis of hand and thigh reveal little or no contributions from the paraffin wax, indicating that the dewaxing procedure has been effective. The characteristic bands of wax [see F in Fig. 6(a)] at 1062, 1131, 1296, and 1441 cm^{-1} are completely absent in the mean spectra of the epidermis of the dewaxed skin hand and thigh [see A and B in Fig. 6(a)]. Hence, the wax contribution of the epidermis has been completely removed by the dewaxing procedure. Notably, however, the mean spectra of dewaxed hand and thigh dermis are devoid of lipidic contributions. Both paraffin wax and biological lipids are long chain aliphatic molecules. The spectra of wax and pure lipids show remarkable resemblances [see F in Fig. 6(a); see C, D, E in Fig. 2(c)]. The Raman contributions of pure lipids at 1064, 1296, and 1442 cm^{-1} in cluster 1 of unprocessed skin hand and thigh [see A and B in Fig. 2(a)] are almost identical to those of pure wax in the wavenumber region of 1000 to 1700 cm^{-1}. The results indicate, therefore, that while the dewaxing procedure is successful in completely removing the wax in the tissue, due to the molecular similarity, the process is also effective in the complete removal of the naturally occurring tissue lipids.

Despite minor differences, the spectra of the clusters corresponding to the dewaxed SC of hand and thigh [see A and B in
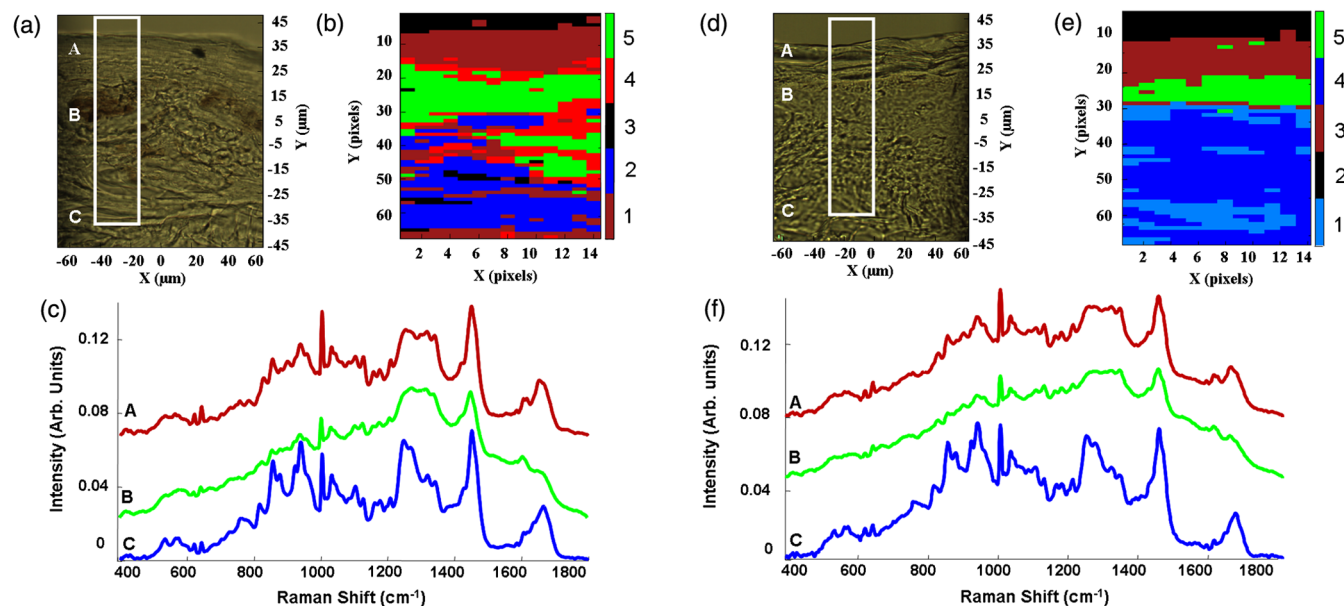

Fig. 5 (a) Optical image of dewaxed hand tissue section; (b) KMCA of Raman spectral map; (c) KMCA mean Raman spectra of processed hand illustrating the differentiation of the superficial SC (cluster 1 = A), the intermediate epithelium (cluster 5 = B), and the dermis (cluster 2 = C); (d) Optical image of processed thigh tissue section; (e) KMCA of Raman map; (f) KMCA mean Raman spectra of processed thigh, illustrating the differentiation of the superficial SC (cluster 3 = A), the intermediate epithelium (cluster 5 = B), and the dermis (cluster 4 = C).
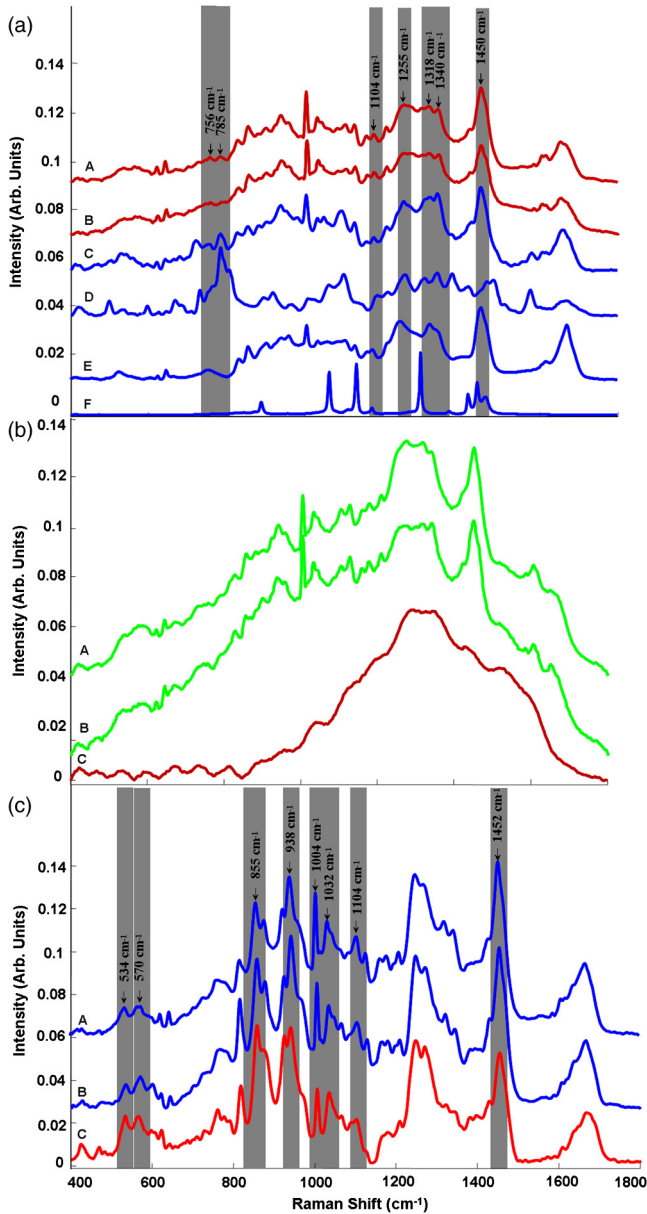
Fig. 6 (a) KMCA mean spectra of cluster 1 from dewaxed skin hand (A) cluster 3 from dewaxed thigh (B), Raman spectra of HaCaT cells (C), DNA (D), histone (E), and pure paraffin wax (F), (b) KMCA mean Raman spectra of cluster 5 from dewaxed skin hand (A), cluster 5 from dewaxed thigh (B), and spectrum of pure melanin (C), (c) KMCA mean Raman spectra of cluster 2 dewaxed skin hand (A) cluster 4 dewaxed thigh (B) pure collagen (C).

Fig. 6(a)] show remarkable resemblances. Protein bands, such as those at 1450 and 1340 cm^{-1} due to protein CH deformation, 1255 cm^{-1} due to protein Amide III, and 756 cm^{-1} due to tryptophan, ring breathing modes are also present in the spectra of HaCaT cells [see C in Fig. 6(a)]. Notably, however, the signature bands of nucleic acids, visible in the spectrum of the HaCaT cells at 785 and 1580 cm^{-1}, are absent in the mean spectrum of the SC.

Although the SC is rich in lipidic components, after dewaxing it is clear that most of the lipids have been lost, and the main molecules contributing to the spectra recorded are the proteins, contained within the corneocytes. Although the lipids of the SC

are widely investigated and often considered as the most important component of the skin, the proteins are also subject to a certain degree of reorganization during the maturation of the keratinocytes from the deepest layers until they reach the surface of the skin. The large, insoluble protein named profilaggrin will be converted to filaggrin which is associated to the keratin filament in the deepest layers of the SC. The proteolysis of filaggrin converts it to its constituent amino acids, and amino-acid derivatives.[70,99] The final form is known as natural moisture factor (NMF), and it can represent up to 10% of the corneocyte dry weight. The complex composition of the NMF mixture can explain the presence of numerous features of the spectrum recorded from the SC. The pattern of the Raman spectra presented in Fig. 6(a) is consistent with data that can be found in the literature focusing on the study of the corneocyte maturation.[90] Moreover, the protein features are highlighted in the absence of the normally strong lipidic spectral features.

Figure 6(b) shows a comparison between cluster 5 of dewaxed hand skin and the equivalent cluster for thigh skin with pure melanin. As described in Sec. 3.3, both clusters [see A and B in Fig. 6(b)] can be attributed to a combination of the basal and malpighian layers of the human skin, both rich in melanin. Again, the intensities of the spectra are exceptionally high, and the spectra are dominated by the fluorescence spectrum of melanin. The spectra are similar to the corresponding spectra from the unprocessed tissue sections [see A and B in Fig. 2(b)]. However, no lipidic peaks are observable and, notably, no differences between the spectra of cluster 5 of dewaxed hand and the equivalent thigh spectrum are apparent [see A and B in Fig. 6(b)]. The process of waxing and dewaxing therefore substantially reduces the lipidic content of the intermediate epithelial layers, such that intermediate epithelial layers from different anatomical sites such as hand and thigh cannot be distinguished from each other.

Figure 6(c) presents a comparison between the KMCA spectra of cluster 2 of dewaxed hand dermis and the equivalent cluster for thigh [see A and B in Fig. 6(c)] with pure collagen [see C in Fig. 6(c)]. As is the case with the epidermis layers, no lipidic peaks are observed. In contrast to the spectra of dermal clusters of unprocessed hand and thigh [see A and B in Fig. 2(a)], the spectra look identical. The process of waxing and dewaxing appears to have removed all lipidic constituents, and therefore the dermis from different anatomical sites such as hand and thigh cannot be distinguished.

The Raman spectra of the stratum corneum and dermis of the dewaxed skin sections from different anatomical regions and from different human cadavers are shown in Fig. 3(a) and 3(b). Remarkably, comparing the Raman spectra of dewaxed epidermis and dermis of human skin from three different cadavers, no significant differences can be found. As in the case of unprocessed sections, the results are representative of all 11 cadavers measured.

To confirm the depletion of the lipidic content of the tissue, Fig. 7 shows the high wavenumber regions of the spectra of dewaxed human thigh SC, intermediate epithelial layer, and dermis. As for the unprocessed sections, the spectra were fitted with a series of Gaussian/Lorentzian bands, and the spectral positioning (± 3 cm^{-1}), intensities ($\pm 10\%$), and assignments are listed in Table 3.

Comparison of the relative intensities of the lipid peaks of unprocessed and processed tissue sections of hand and thigh in Tables 2 and 3 confirms that the dewaxing procedure has
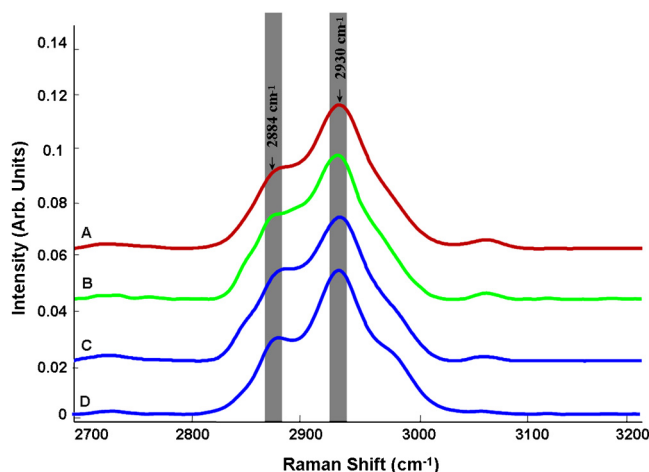
Fig. 7 Average Raman spectra of the high wavenumber region of dewaxed human thigh section from SC (A), intermediate epithelial layer (B), dermis (C), and pure collagen (D).

Table 3 Fitted peak positions, intensities and assignments for high wavenumber region of average Raman spectra of dewaxed thigh skin section.

Peak position (cm^{-1})	Stratum corneum	Dermis	Intermediate epithelium	Assignment
2730	0.05	0.04	0.04	CH stretching (lipid)
2850	0.17	0.18	0.35	CH_2 stretching (lipid)
2863	0.59	0.28	0.63	CH_3 stretching (protein)
2880	0.02	0.16	0.09	CH_2 stretching (lipid)
2905	0.87	0.57	0.93	CH stretching (protein)
2933	1	1	1	CH_3 stretching (protein)
2968	0.69	0.49	0.79	CH_3 stretching (protein)
3065	0.10	0.02	0.07	Amide B (protein) (CNH bend)

significantly reduced the lipidic content and altered the tissue composition of the skin. Strikingly, however, the remaining biochemical structure of the skin layers is remarkably consistent across different cadavers and anatomical sites.

The lipidic content is the key to the permeability barrier function of skin and is of significant importance to the cosmetics industry and for transdermal drug delivery. Abnormalities in barrier function associated with lipid content are also associated with atopic dermatitis and other common cutaneous diseases.[100] UV radiation has been shown to effect the free fatty acid and

triglyceride composition,[101] and decrease in lipid content with age is associated with increased susceptibility to exogenous insults.[94] Therefore, a detailed knowledge of lipidic content, composition, and structure is critical to many studies of skin function, malfunction, and abnormality. Although archived tissue samples can serve as an important source for retrospective studies, this study demonstrates that, in their dewaxed form, no information related to their lipid content can be gleaned. Nevertheless, the study shows that the cellular content of the tissue and the protein extracellular matrix remain largely intact, and that the spectral profiles are enhanced by the removal of the lipidic content.

4 Conclusions

Raman spectroscopy and KMCA successfully discriminates the layers of the unprococessed and dewaxed skin from two different anatomical sites, hand and thigh. KMCA further shows that distinct biochemcial regions within the skin tissue can be identified, corresponding to the top layer SC and the bottom layer dermis. However, the strong contribution from melanin fluoresecene prevents a clear discrimination between the stratum basale and stratum spinosum. In the unprocessed skin, the spectrum of the SC has strong contributions from the cellular components; the spectrum of the intermediate epithelial layer is strongly influenced by melanin while that of the dermis is dominated by collagen. In all cases, lipidic contibutions to the spectra are discernible, notably in the SC, which is relatively rich in lipidic content. The lipidic content can also be used to differentiate between anatomical sites. The process of tissue fixation, embedding, and dewaxing has the effect of significantly reducing the lipidic content of all skin layers. This has the implication that antomically different tissue sections which may differ significantly in terms of fat content become indistinguishable, and it is no longer possible to study skin functions or abnormalities accociated with lipid content. However, the cellular and extracellular structures remain relatively intact and the spectral features are accentuated in the absence of lipidic contributions, and so processed archived tissue banks present a valuable resource for the retrospective study of skin diesase.

References

1. A. D. Meade, H. J. Byrne, and F. M. Lyng, "Spectroscopic and chemometric approaches to radiobiological analyses," *Mutat. Res* **704**(1–3), 108–114 (2010).
2. P. Knief et al., "Raman spectroscopy—a potential platform for the rapid measurement of carbon nanotube-induced cytotoxicity," *Analyst* **134**(6), 1182–1191 (2009).
3. J. Ling et al., "Direct Raman imaging techniques for study of the subcellular distribution of a drug," *Appl. Opt.* **41**(28), 6006–6017 (2002).
4. D. Sebiskveradze et al., "Automation of an algorithm based on fuzzy clustering for analyzing tumoral heterogeneity in human skin carcinoma tissue sections," *Lab Invest* **91**(5), 799–811 (2011).
5. R. Wolthuis et al., "IR spectral imaging for histopathological characterization of xenografted human colon carcinomas," *Anal. Chem.* **80**(22), 8461–8469 (2008).

6. H. Nawaz et al., "Evaluation of the potential of Raman microspectroscopy for prediction of chemotherapeutic response to cisplatin in lung adenocarcinoma," *Analyst* **135**(12), 3070–3076 (2010).

7. F. Draux et al., "IR spectroscopy reveals effect of non-cytotoxic doses of anti-tumour drug on cancer cells," *Anal. Bioanal. Chem.* **395**(7), 2293–2301 (2009).

8. F. Bonnier et al., "Imaging live cells grown on a three dimensional collagen matrix using Raman microspectroscopy," *Analyst* **135**(12), 3169–3177 (2010).

9. M. Miljkovic et al., "Label-free imaging of human cells: algorithms for image reconstruction of Raman hyperspectral datasets," *Analyst* **135**(8), 2002–2013 (2010).

10. A. Mahadevan-Jansen et al., "Near-infrared Raman spectroscopy for in vitro detection of cervical precancers," *Photochem. Photobiol.* **68**(1), 123–132 (1998).

11. U. Utzinger et al., "Reflectance spectroscopy for in vivo characterization of ovarian tissue," *Lasers Surg. Med.* **28**(1), 56–66 (2001).

12. Z. Huang et al., "Near-infrared Raman spectroscopy for optical diagnosis of lung cancer," *Int. J. Cancer* **107**(6), 1047–1052 (2003).

13. S. Kaminaka et al., "Near-infrared Raman spectroscopy of human lung tissues: possibility of molecular-level cancer diagnosis," *J. Raman Spectrosc.* **32**(2), 139–141 (2001).

14. A. Mizuno et al., "Near-infrared Fourier transform Raman spectroscopic study of human brain tissues and tumours," *J. Raman Spectrosc.* **25**(1), 25–29 (1994).

15. I. A. Boere et al., "Monitoring in situ dosimetry and protoporphyrin IX fluorescence photobleaching in the normal rat esophagus during 5-aminolevulinic acid photodynamic therapy," *Photochem. Photobiol.* **78**(3), 271–277 (2003).

16. C. Kendall et al., "Raman spectroscopy, a potential tool for the objective identification and classification of neoplasia in Barrett's oesophagus," *J. Pathol.* **200**(5), 602–609 (2003).

17. I. A. Boere et al., "Use of fibre optic probes for detection of Barrett's epithelium in the rat oesophagus by Raman spectroscopy," *Vib. Spectrosc.* **32**(1), 47–55 (2003).

18. A. Molckovsky et al., "Diagnostic potential of near-infrared Raman spectroscopy in the colon: differentiating adenomatous from hyperplastic polyps," *Gastrointest. Endosc.* **57**(3), 396–402 (2003).

19. C. Krafft et al., "Raman and FTIR microscopic imaging of colon tissue: a comparative study," *J. Biophotonics* **1**(2), 154–169 (2008).

20. P. Crow et al., "The use of Raman spectroscopy to identify and grade prostatic adenocarcinoma in vitro," *Br. J. Cancer* **89**(1), 106–108 (2003).

21. D. P. Lau et al., "Raman spectroscopy for optical diagnosis in normal and cancerous tissue of the nasopharynx-preliminary findings," *Lasers Surg. Med.* **32**(3), 210–214 (2003).

22. D. P. Lau et al., "Raman spectroscopy for optical diagnosis in the larynx: preliminary findings," *Lasers Surg Med* **37**(3), 192–200 (2005).

23. C. M. Krishna et al., "Micro-Raman spectroscopy for optical pathology of oral squamous cell carcinoma," *Appl. Spectrosc.* **58**(9), 1128–1135 (2004).

24. C. J. Frank, R. L. McCreery, and D. C. Redd, "Raman spectroscopy of normal and diseased human breast tissues," *Anal. Chem.* **67**(5), 777–783 (1995).

25. K. E. Shafer-Peltier et al., "Model-based biological Raman spectral imaging," *J. Cell Biochem. Suppl.* **39**, 125–137 (2002).

26. K. E. Shafer-Peltier et al., "Raman microspectroscopic model of human breast tissue: implications for breast cancer diagnosis in vivo," *J. Raman Spectrosc.* **33**(7), 552–563 (2002).

27. H. Abramczyk et al., "The label-free Raman imaging of human breast cancer," *J. Mol. Liq.* **164**, 123–131 (2011).

28. S. R. Hawi et al., "Characterization of normal and malignant human hepatocytes by Raman microspectroscopy," *Cancer Lett* **110**(1–2), 35–40 (1996).

29. E. Ly et al., "Differential diagnosis of cutaneous carcinomas by infrared spectral micro-imaging combined with pattern recognition," *Analyst* **134**(6), 1208–1214 (2009).

30. E. Ly et al., "Combination of FTIR spectral imaging and chemometrics for tumour detection from paraffin-embedded biopsies," *Analyst* **133**(2), 197–205 (2008).

31. P. J. Caspers et al., "In vivo confocal Raman microspectroscopy of the skin: noninvasive determination of molecular concentration profiles," *J. Invest. Dermatol.* **116**(3), 434–442 (2001).

32. A. Nijssen et al., "Discriminating basal cell carcinoma from its surrounding tissue by Raman spectroscopy," *J Invest Dermatol* **119**(1), 64–69 (2002).

33. E. Ly et al., "Polarized Raman microspectroscopy can reveal structural changes of peritumoral dermis in basal cell carcinoma," *Appl. Spectrosc.* **62**(10), 1088–1094 (2008).

34. M. Wegenera et al., "Structure of stratum corneum lipids characterized by FT-Raman spectroscopy and DSC. I. ceramides," *Int. J. Pharm.* **128**, 203–213 (1996).

35. A. Tfayli et al., "Thermal dependence of Raman descriptors of ceramides. Part I: effect of double bonds in hydrocarbon chains," *Anal. Bioanal. Chem.* **397**(3), 1281–1296 (2010).

36. J. D. Bancroft and M. Gamble, *Theory and Practice of Histological Techniques*, Churchill Livingstone, London (2002).

37. R. Drury and E. Wallington, *Carleton's Histological Technique*, Oxford University Press, Oxford (1980).

38. E. O. Faolain et al., "Raman spectroscopic evaluation of efficacy of current paraffin wax section dewaxing agents," *J. Histochem. Cytochem.* **53**(1), 121–129 (2005).

39. A. Tfayli et al., "Digital dewaxing of Raman signals: discrimination between nevi and melanoma spectra obtained from paraffin-embedded skin biopsies," *Appl. Spectrosc.* **63**(5), 564–570 (2009).

40. F. Draux et al., "Raman spectral imaging of single cancer cells: probing the impact of sample fixation methods," *Anal. Bioanal. Chem.* **397**(7), 2727–2737 (2010).

41. M. M. Mariani et al., "Impact of fixation on in vitro cell culture lines monitored with Raman spectroscopy," *Analyst* **134**(6), 1154–1161 (2009).

42. A. Meade et al., "Studies of chemical fixation effects in human cell lines using Raman microspectroscopy," *Anal. Bioanal. Chem.* **396**(5), 1781–1791 (2010).

43. P. Boukamp et al., "Normal keratinization in a spontaneously immortalized aneuploid human keratinocyte cell line," *J. Cell Biol.* **106**(3), 761–771 (1988).

44. H. M. Ockenfels et al., "Cyclosporin A, FK506 and dithranol after tyrosine-specific protein phosphorylation in HaCaT keratinocytes," *Arch. Dermatol. Res.* **287**(3–4), 304–309 (1995).

45. S. J. Choquette et al., "Relative intensity correction of Raman spectrometers: NIST SRMs 2241 through 2243 for 785 nm, 532 nm, and 488 nm/514.5 nm excitation," *Appl. Spectrosc.* **61**(2), 117–129 (2007).

46. F. Bonnier et al., "In vitro analysis of immersed human tissues by Raman microspectroscopy," *J. Raman Spectrosc.* **42**(5), 888–896 (2011).

47. S. Koljenovic et al., "Raman microspectroscopic mapping studies of human bronchial tissue," *J. Biomed. Opt.* **9**(6), 1187–1197 (2004).

48. P. J. Caspers et al., "In vitro and in vivo Raman spectroscopy of human skin," *Biospectroscopy* **4**(5), S31–S39 (1998).

49. A. Tfayli et al., "Discriminating nevus and melanoma on paraffin-embedded skin biopsies using FTIR microspectroscopy," *Biochim. Biophys. Acta* **1724**(3), 262–269 (2005).

50. F. H. Silver, J. W. Freeman, and D. DeVore, "Viscoelastic properties of human skin and processed dermis," *Skin Res. Technol.* **7**(1), 18–23 (2001).

51. B. G. Frushour and J. L. Koenig, "Raman scattering of collagen, gelatin, and elastin," *Biopolymers* **14**(2), 379–391 (1975).

52. J. De Gelder et al., "Raman spectroscopic study of bacterial endospores," *Anal. Bioanal. Chem.* **389**(7–8), 2143–2151 (2007).

53. P. R. Jess et al., "Early detection of cervical neoplasia by Raman spectroscopy," *Int. J. Cancer* **121**(12), 2723–2728 (2007).

54. I. Notingher and L. L. Hench, "Raman microspectroscopy: a noninvasive tool for studies of individual living cells in vitro," *Expert Rev. Med. Dev.* **3**(2), 215–234 (2006).

55. I. Notingher et al., "Spectroscopic study of human lung epithelial cells (A549) in culture: living cells versus dead cells," *Biopolymers* **72**(4), 230–240 (2003).

56. A. Tfayli et al., "Molecular characterization of reconstructed skin model by Raman microspectroscopy: comparison with excised human skin," *Biopolymers* **87**(4), 261–274 (2007).

57. N. T. Kollias, "The physical basis of skin color and its evaluation," *T. Clin. Dermatol.* **13**, 361–367 (1995).

58. G. F. Odland in *Physiology, Biochemistry and Molecular Biology of the Skin*, L. A. Goldsmith, Ed., 2nd ed., pp. 3–62, Oxford University Press, New York (1991).

59. N. G. Jablonski, "The evolution of human skin and skin colour," *Annu. Rev. Anthropol.* **33**, 585–623 (2004).

60. Z. Huang et al., "Raman spectroscopy of in vivo cutaneous melanin," *J Biomed. Opt.* **9**(6), 1198–1205 (2004).

61. A. C. Williams et al., "A critical comparison of some Raman-spectroscopic techniques for studies of human stratum-corneum," *Pharm. Res.* **10**(11), 1642–1647 (1993).

62. A. C. Williams, H. G. M. Edwards, and B. W. Barry, "Fourier-transform Raman-spectroscopy a novel application for examining human stratum-corneum," *Int. J. Pharm.* **81**(2–3), R11–R14 (1992).

63. B. W. Barry, H. G. M. Edwards, and A. C. Williams "Fourier-transform Raman and infrared vibrational study of human skin—assignment of spectral bands," *J. Raman Spectrosc.* **23**(11), 641–645 (1992).

64. H. G. M. Edwards et al., "Novel spectroscopic deconvolution procedure for complex biological-systems—vibrational components in the FT-Raman spectra of ice-man and contemporary skin," *J. Chem. Soc.-Faraday Transactions* **91**(21), 3883–3887 (1995).

65. A. N. C. Anigbogu et al., "Fourier-transform Raman-spectroscopy of interactions between the penetration enhancer dimethyl-sulfoxide and human stratum-corneum," *Int. J. Pharm.* **125**(2), 265–282 (1995).

66. R. O. Potts et al., "A noninvasive, in vivo technique to quantitatively measure water concentration of the stratum corneum using attenuated total-reflectance infrared spectroscopy," *Arch. Dermatol. Res.* **277**(6), 489–495 (1985).

67. I. Plasencia, L. Norlen, and L. A. Bagatolli, "Direct visualization of lipid domains in human skin stratum corneum's lipid membranes: effect of pH and temperature," *Biophys. J.* **93**(9), 3142–3155 (2007).

68. M. A. Lampe et al., "Human stratum corneum lipids: characterization and regional variations," *J. Lipid Res.* **24**(2), 120–130 (1983).

69. B. C. Melnik et al., "Microanalytical screening of all major stratum corneum lipids by sequential high-performance thin-layer chromatography," *J. Invest. Dermatol.* **92**(2), 231–234 (1989).

70. C. R. Harding et al., "Dry skin, moisturization and corneodesmolysis," *Int. J. Cosmet. Sci.* **22**(1), 21–52 (2000).

71. M. E. Darvin et al., "In vivo distribution of carotenoids in different anatomical locations of human skin: comparative assessment with two different Raman spectroscopy methods," *J. Exp. Dermatol.* **18**(12), 1060–1063 (2009).

72. N. I. Krinsky, "Carotenoids as antioxidants," *Nutrition* **17**(10), 815–817 (2001).

73. J. Lademann et al., "Interaction between carotenoids and free radicals in human skin," *Skin Pharmacol. Physiol.* **24**(5), 238–244 (2011).

74. J. P. Hulsbergen Henning, E. G. Beerens, and J. C. van der Leun, "A non-invasive microscopic method for measuring epidermal thickness in vivo," *Arch. Dermatol. Res.* **258**(1), 25–32 (1977).

75. P. Corcuff and J. L. Leveque, "In vivo vision of the human skin with the tandem scanning microscope," *Dermatology* **186**(1), 50–54 (1993).

76. A. M. Kligman, *The Epidermis: The Biology of Stratum corneum*, pp. 407–408, Academic Press, New York (1964).

77. J. T. Whitton and J. D. Everall, "The thickness of the epidermis," *Br. J. Dermatol.* **89**(5), 467–476 (1973).

78. K. A. Holbrook and G. F. Odland, "Regional differences in the thickness (cell layers) of the human stratum corneum: an ultrastructural analysis," *J. Invest. Dermatol.* **62**(4), 415–422 (1974).

79. M. Huzaira et al., "Topographic variations in normal skin, as viewed by in vivo reflectance confocal microscopy," *J. Invest. Dermatol.* **116**(6), 846–852 (2001).

80. K. Robertson and J. L. Rees, "Variation in epidermal morphology in human skin at different body sites as measured by reflectance confocal microscopy," *Acta. Derm. Venereol.* **90**(4), 368–373 (2010).

81. J. Sandby-Moller, T. Poulsen, and H. C. Wulf, "Epidermal thickness at different body sites: relationship to age, gender, pigmentation, blood content, skin type and smoking habits," *Acta. Derm. Venereol* **83**(6), 410–413 (2003).

82. M. Gniadecka et al., "Structure of water, proteins, and lipids in intact human skin, hair, and nail," *J. Invest. Dermatol.* **110**(4), 393–398 (1998).

83. M. Gniadecka et al., "Water and protein structure in photoaged and chronically aged skin," *J Invest Dermatol* **111**(6), 1129–1133 (1998).

84. A. S. Michaels, S. K. Chandrasekaran, and J. E. Shaw, "Drug permeation through human skin—theory and in vitro experimental measurement," *Aiche J.* **21**(5), 985–996 (1975).

85. S. Grayson and P. M. Elias, "Isolation and lipid biochemical-characterization of stratum-corneum membrane complexes—implications for the cutaneous permeability barrier," *J. Invest. Dermatol.* **78**(2), 128–135 (1982).

86. P. W. Wertz and D. T. Downing, "Glycolipids in mammalian epidermis: structure and function in the water barrier," *Science* **217**(4566), 1261–1262 (1982).

87. P. W. Wertz, "The nature of the epidermal barrier: biochemical aspects," *Adv. Drug Deliv. Rev.* **18**(3), 283–294 (1996).

88. P. W. Wertz and B. van den Bergh, "The physical, chemical and functional properties of lipids in the skin and other biological barriers," *Chem. Phys. Lipids* **91**(2), 85–96 (1998).

89. J. M. Jungersted et al., "Lipids and skin barrier function—a clinical perspective," *Contact Dermatitis* **58**(5), 255–262 (2008).

90. G. Zhang et al., "Vibrational microscopy and imaging of skin: from single cells to intact tissue," *Anal. Bioanal. Chem.* **387**(5), 1591–1599 (2007).

91. P. W. Wertz and D. T. Downing in *Physiology, Biochemistry and Molecular Biology of the Skin: Epidermal Lipids*, L. A. Goldsmith, Ed., pp. 205–236, Oxford University Press, New York (1991).

92. D. T. Downing, "Lipid and protein structures in the permeability barrier of mammalian epidermis," *J. Lipid Res.* **33**(3), 301–313 (1992).

93. Y. Mizutani et al., "Ceramide biosynthesis in keratinocyte and its role in skin function," *Biochimie* **91**(6), 784–790 (2009).

94. R. Ghadially et al., "The aged epidermal permeability barrier—structural, functional, and lipid biochemical-abnormalities in humans and a senescent murine model," *J. Clin. Invest.* **95**(5), 2281–2290 (1995).

95. E. Guillard et al., 'Thermal dependence of Raman descriptors of ceramides. Part II: effect of chains lengths and head group structures," *Anal. Bioanal. Chem.* **399**(3), 1201–1213 (2011).

96. C. Merle, C. Laugel, and A. Baillet-Guffroy, 'Effect of UVA or UVB irradiation on cutaneous lipids in films or in solution," *Photochem. Photobiol.* **86**(3), 553–562 (2010).

97. A. Tfayli et al., "Raman spectroscopy: feasibility of in vivo survey of stratum corneum lipids, effect of natural aging," *Eur. J. Dermatol.* **22**(1), 36–41 (2012).

98. C. Gobinet et al., 'Pre-processing and source separation methods for Raman spectra analysis of biomedical samples," *Conf Proc IEEE Eng Med Biol Soc*, Vol. **2007**, 6208–6211 (2007).

99. I. R. Scott and C. R. Harding, "Filaggrin breakdown to water binding compounds during development of the rat stratum corneum is controlled by the water activity of the environment," *Dev. Biol.* **115**(1), 84–92 (1986).

100. K. R. Feingold, "The importance of lipids in cutaneous function," *J. Lipid Res.* **48**(12), 2529–2530 (2007).

101. E. J. Kim et al., "UV decreases the synthesis of free fatty acids and triglycerides in the epidermis of human skin in vivo, contributing to development of skin photoaging," *J. Dermatol. Sci.* **57**(1), 19–26 (2010).